Journal of Alloys and Compounds 555 (2013) 39–44

Contents lists available at SciVerse ScienceDirect

Journal of Alloys and Compounds

journal homepage: www.elsevier.com/locate/jalcom

Structural characterization and electrical properties of sintered magnesium–titanate ceramics

S. Filipović [a], N. Obradović [a,*], J. Krstić [b], M. Šćepanović [c], V. Pavlović [a], V. Paunović [d], M.M. Ristić [e]

[a] Institute of Technical Sciences-SASA, Knez Mihajlova 35/IV, 11000 Belgrade, Serbia
[b] University of Belgrade, Institute of Chemistry, Technology and Metallurgy, Department of Catalysis and Chemical Engineering, Njegoševa 12, 11000 Belgrade, Serbia
[c] Institute of Physics, University of Belgrade, Pregrevica 118, 11080 Belgrade, Serbia
[d] Faculty for Electronics, University of Niš, Aleksandra Medvedeva 14, 18000 Niš, Serbia
[e] Serbian Academy of Sciences and Arts, Knez Mihajlova 35, 11000 Belgrade, Serbia

ARTICLE INFO

Article history:
Received 27 August 2012
Received in revised form 5 December 2012
Accepted 11 December 2012
Available online 20 December 2012

Keywords:
Ball milling
SEM
Raman spectroscopy
Sintering
Titanates

ABSTRACT

In this article the influence of ball miling process on structure of $MgO–TiO_2$ system, as well as the electrical properties of samples after sintering, was investigated. The mixtures of $MgO–TiO_2$ powders were mechanically activated in a planetary ball mill for the time period from 0 to 120 min. The influence of mechanical activation and sintering on the lattice vibrational spectra was studied by Raman spectroscopy at room temperature. Structural investigations have been performed on produced powders. Nitrogen adsorption method was used to determine the BET specific surface area and pore size distribution. Unusual results have been obtained: specific surface area continuosly decreased up to 40 min of activation and increased after that, reaching its minimun value of 5.5 m^2/g. The Raman spectra of activated powders have shown that anatase modes have been decreasing in intensity and broadening as the time of activation extended. Also, the additional modes attributed to TiO_2 II, srilankite and rutile phases started to appear as a consequence of activation. The small differences noticed in the Raman spectra of sintered samples have been explained by structural modification of $MgTiO_3$ phase due to the presence of defects.

The effects of activation and sintering process on microstructure were investigated by scanning electron microscopy (SEM). The electrical measurements showed difference in dielectric constant (ε_r), loss tangent ($tg\delta$) and specific resistance (ρ) as a function of time of mechanical treatment.

1. Introduction

Many recent investigations were based on development of materials with low dielectric loss in microwave range, because of their wide usage in modern communication devices, such as cellular telephones, antennas, and global positioning systems [1–4]. From this point of view, low-cost dielectric materials with dielectric constant of 10–20 and low dielectric losses are required. In the binary system of $MgO–TiO_2$, two magnesium–titanates are known, $MgTiO_3$ and Mg_2TiO_4, both good for applications mentioned above. These compounds have dielectric constant $\varepsilon = 16$ and $\varepsilon = 14$, respectively [5]. Moreover, the influence of the molar ratio of these phases on dielectric constant is registered [6]. The $MgTiO_3$, geikiete (rhombohedra of ilmenite structure with space group $R\bar{3}$), is formed above 600 °C and it is stable in the range from room temperature to its melting point [7,8]. The Mg_2TiO_4 (cubic of inverse spinel type with space group $Fd\bar{3}m$) is formed at temperatures above 1150 °C and undergo a phase transition in the process of cooling at ~1000 °C to a tetragonal modification (space group $P4_122$) [9].

So far, many methods for the preparation of $MgTiO_3$ and Mg_2TiO_4 were reported in literature, such as thermal decomposition of peroxide precursors, hydrothermal mechano-chemical complexation routes, sol–gel routes, auto-ignited method, chemical coprecipitation and metalorganic solution deposition technique [4,10]. The solid-state reaction by grinding in mill is often used method, due to its simplicity, inexpensiveness, applicability, etc. In addition, it is well known that mechanical activation could simplify or accelerate solid-state reaction, reducing temperatures of chemical reaction or sintering temperature [11]. The intention of this work was to determine influence of mechanical treatment on structure of milling mixtures and changes in electrical properties of sintered samples.

2. Experimental procedure

Starting components were MgO (99% Sigma–Aldrich) and TiO_2 powders (99.8% Sigma–Aldrich). Mixtures at a molar ratio $MgO:TiO_2 = 2:1$ and ball to powder mixture mass ratio 20:1 were mechanically activated in a high energy planetary ball mill device (Retsch type PH 100), with zirconia-oxide vials and balls. Milled pow-

* Corresponding author. Tel./fax: +381 11 2185 263.
E-mail address: obradovic.nina@yahoo.com (N. Obradović).

0925-8388/$ - see front matter © 2012 Elsevier B.V. All rights reserved.
http://dx.doi.org/10.1016/j.jallcom.2012.12.040

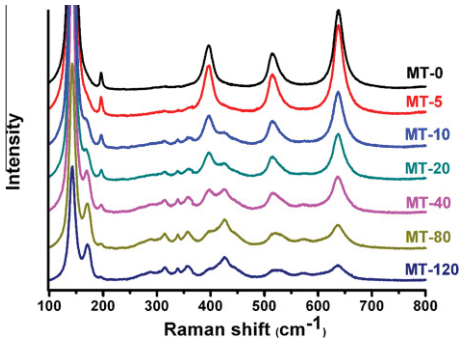

Fig. 1. Raman spectra of non-milled and ball milled powders. Some spectra are upshifted for clarity.

ders have been labeled as MT-*t*, where *t* denoted the time of milling, and MTS-*t*, for sintered samples. The morphology of obtained powders have been investigated by scanning electron microscopy (JEOL JSM-6390 LV). Textural characteristics of starting $MgO:TiO_2$ mixture and milled powder, were determined by N_2 physisoprtion method. Measurements were carried out using a Sorptomatic 1990 Thermo Finnigan at −196 °C temperature after outgassing pretreatment of the samples at 110 °C for 18 h.

The binder-free powders were compacted using the uniaxial double action pressing process under pressure of 392 MPa in an 8 mm diameter tool (Hydraulic press Ring, P-14, Veb Thuringer). The compacts were placed in an alumna boat and heated in a tube furnace (Lenton Thermal Design Type 1600) and sintered isothermally at 1300 °C in air atmosphere for 2 h and the heating rate of 10 °C min^{-1}. The density of specimens was calculated from the measurements of their diameter, thickness and mass.

The Raman scattering measurements of powders and sintered pellets were performed by a TriVista TR557 triple spectrometer equipped with a nitrogen-cooled CCD detector. The spectra were collected in backscattering micro-Raman configuration using 514 nm line of a mixed Ar^+/Kr^+ laser with output power 30 mW. Measurements were carried out in the range of 100–1500 cm^{-1} at room temperature.

The measurements of specific electrical resististance, capacitance and loss tangent of samples were performed in the frequency range from 20 Hz to 1 MHz with a LCR meter Agilent 4284A, on sintered specimens coated with silver electrodes.

3. Results and discussion

There are three different polymorphs of TiO_2 at ambient conditions: body-centered tetragonal structure of *anatase* (space group $I4_1/amd$), orthorhombic *brookite* (*Pbca*), and tetragonal *rutile* ($P4_2/mnm$). According to the factor group analyses there are six Raman active modes in anatase ($A_{1g} + 2B_{1g} + 3E_g$) [12], four Raman active modes in rutile ($A_{1g} + B_{1g} + B_{2g} + E_g$) [13], whereas 36 vibrational bands are predicted in brookite phase [14]. Besides, TiO_2 has two

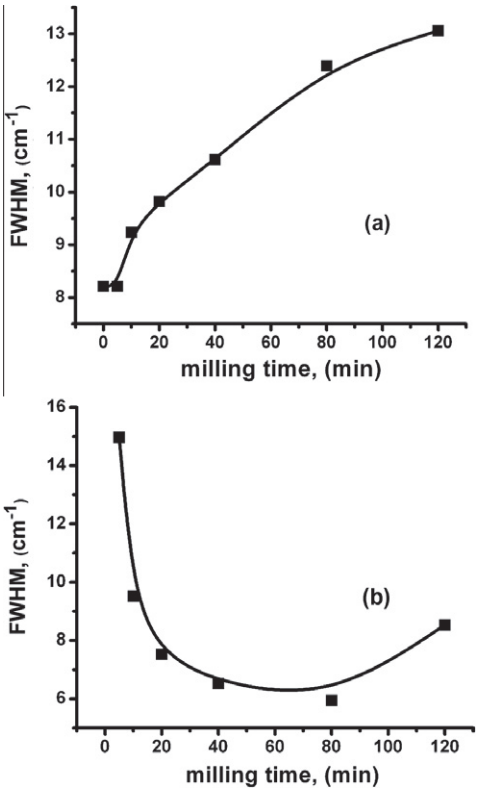

Fig. 2. (a) FWHM for anatase $E_{g(1)}$ Raman mode at ∼142 cm^{-1} as a function of milling time. (b) FWHM for TiO_2 II mode at ∼338 cm^{-1} as a function of milling time.

Table 1
Position and assignments of all observed bends.

Sample	Position and assignments																		
MT-0	143 ■	-	196 ■	-	-	-	-	-	-	-	396 ■	-	-	-	515 ■	-	-	-	-	637 ■
MT-5	142 ■	-	196 ■	-	-	-	314 ▲	-	-	361 ▲	397 ■	-	-	-	515 ■	-	-	-	-	638 ■
MT-10	142 ■	170 ▲	196 ■	-	-	-	314 ▲	338 ▲	-	360 ▲	396 ■	-	425 ▲	447 ▲	514 ■	-	-	-	-	637 ■
MT-20	142 ■	170 ▲	197 ■	-	-	-	315 ▲	338 ▲	-	359 ▲	396 ■	-	425 ▲	448 ▲	518 ■	-	-	-	-	637 ■
MT-40	142 ■	170 ▲	197 ■	267 ▲	287 ▲	310 ▲	315 ▲	339 ▲	-	357 ▲	397 ■	-	425 ▲	448 ▲	514 ■	525 ▲	-	576 ▲	-	637 ■
MT-80	142 ■	174 ▲	198 ■	270 ▲	287 ▲	312 ▲	315 ▲	339 ▲	355 ◊	359 ▲	397 ■	414 ◊	426 ▲	446 ▲	-	522 ▲	-	574 ▲	606 ▶	637 ■
MT-120	142 ■	174 ▲	199 ■	271 ▲	287 ▲	312 ▲	315 ▲	338 ▲	356 ◊	362 ▲	398 ■	415 ◊	428 ▲	448 ▲	-	523 ▲	568 ▲	574 ▲	605 ▶	637 ■

■-anatase, ▲-TiO_2 II, ◊- srilankite, ▶- rutil

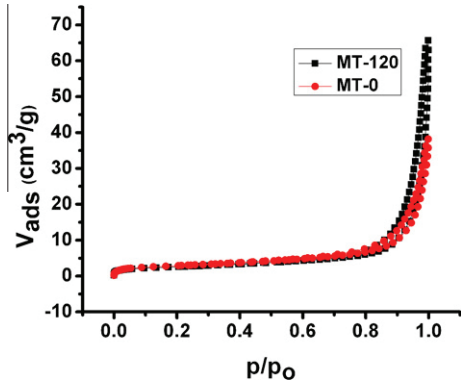

Fig. 3. Nitrogen adsorption/desorption isotherms for the samples MT-0 and MT-120.

Table 2
Results obtained by N_2 sorption.

Sample	S_{BET} (m^2/g)	V_{tot} (cm^3/g)	V_{mes} (cm^3/g)
MT-0	15.8	0.051	0.047
MT-5	10.4	0.038	0.033
MT-10	7.7	0.026	0.024
MT-20	6.4	0.034	0.037
MT-40	5.5	0.029	0.031
MT-80	7.8	0.033	0.034
MT-120	9.2	0.048	0.054

high-pressure phases: TiO_2 II with orthorhombic structure (space group*Pbcn*), and monoclinic srilankite ($P2_1/c$) [15]. At the pressure higher than 2.56 GPa, TiO_2 II is irreversibly formed from anatase and rutile [16]. On the other side, MgO, as a cubic crystal with inversion symmetry, has no first-order Raman active modes [17].

The Raman spectra of non-milled powders and those milled for different time intervals in the range of 100–800 cm^{-1} are shown in Fig. 1. All Raman modes in the spectra of non-milled powder can be assigned to the Raman active modes of anatase crystal [12] as follows: ~143 cm^{-1} ($E_{g(1)}$), 196 cm^{-1} ($E_{g(2)}$), 396 cm^{-1} ($B_{1g(1)}$), 515 cm^{-1} (combination of A_{1g} and $B_{1g(2)}$ that cannot be resolved at room temperature [18]) and 637 cm^{-1} ($E_{g(3)}$). The anatase modes are dominant in Raman spectra of all activated powders, although their intensities decrease and widths increase as the time of activation extended.

In addition to anatase modes, barely noticeable a few new bands between 300 and 400 cm^{-1} in Raman spectra of MT-5 quite visible in MT-10 spectra, can be assigned to TiO_2 II phase [16]. In the Raman spectra of the powders activated for more than 80 min, the weak shoulders, which can be assigned to srilankite and rutile phases [16,19], are also present. The position of all observed Raman modes obtained by deconvolution of the Raman spectra into a series of separated Lorentzian shape peaks using last–squares optimization method, as well as their assignations, are summarized in the Table 1. As it can be seen, there are no significant shifts in the bend positions. Small blue shifts with extended activation time, noticed for the $E_{g(2)}$ anatase mode at ~196 cm^{-1} and TiO_2 II modes at ~170 and ~267 cm^{-1}, most probably are the consequence of the variation in crystal position of oxygen atoms, as well as increased nonstoichiometry and lattice strain introduced by mechanical treatment.

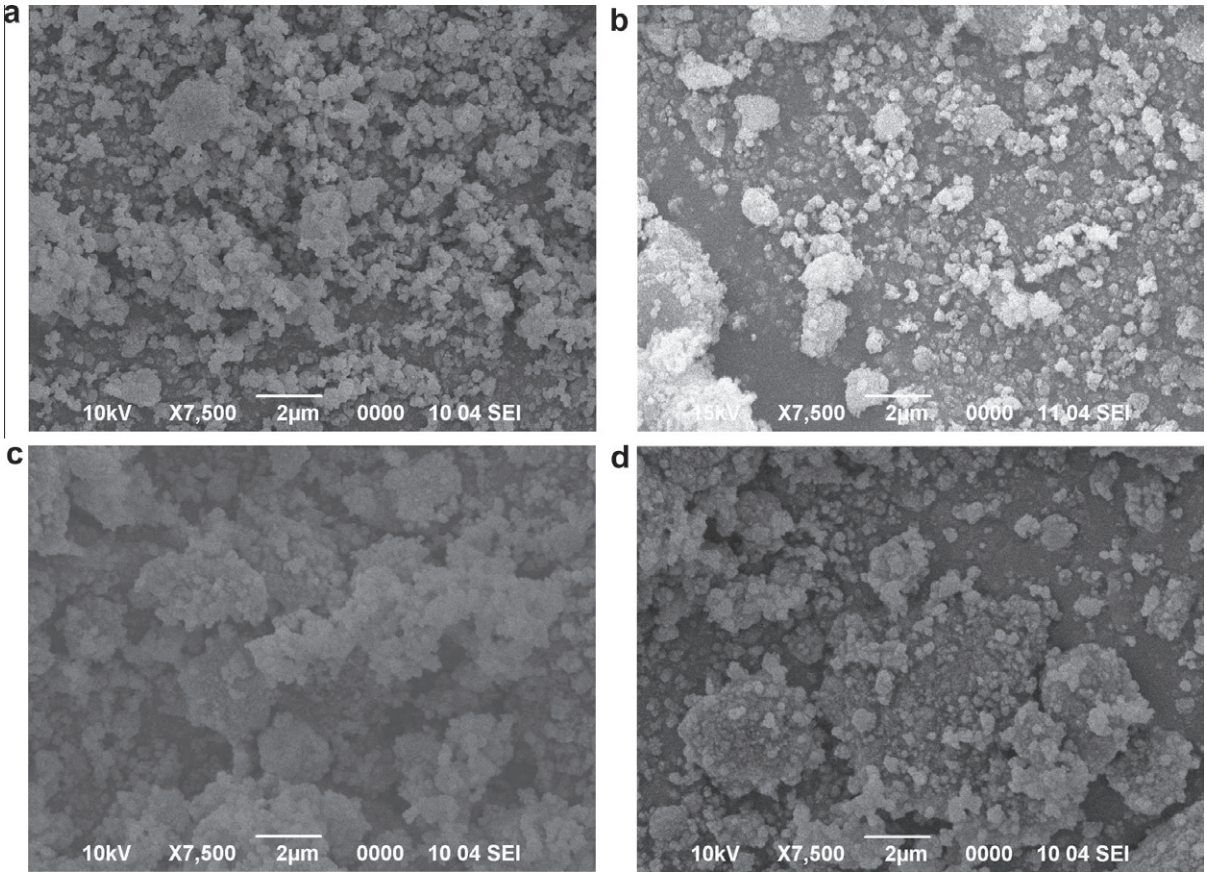

Fig. 4. Scanning electron micrographs of the samples (a) MT-0, (b) MT-10, (c) MT-40 and (d) MT-80.

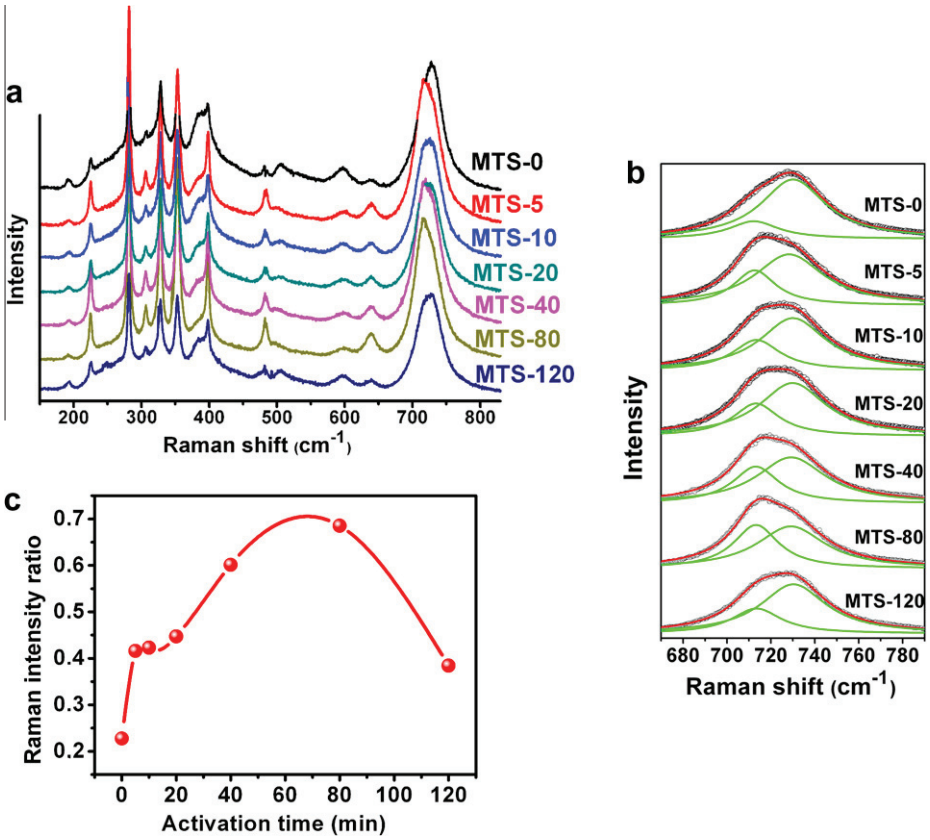

Fig. 5. (a) Raman spectra of samples sintered at 1300 °C. Some spectra are up-shifted for clarity. (b) Raman feature at about 730 cm^{-1} (o) fitted by a sum (thick lines) of two Lorentzian peaks (thin lines). (c) Intensity ratio of Lorentzian peaks at ~713 and ~730 cm^{-1}. The line is just a guide for the eye.

Table 3
Electrical properties of sintered samples at 1 MHz frequency.

Sample	ε_r	$tg\delta \cdot 10^{-3}$	$\rho \cdot 10^6(\Omega cm)$	d (% d_t)
MT-0–1300	29.3	9.37	3.43	84.17
MT-5–1300	31.2	8.54	3.90	87.76
MT-10–1300	30.7	8.40	3.99	88.45
MT-20–1300	29.0	8.43	4.24	88.35
MT-40–1300	30.0	8.24	4.28	89.79
MT-80–1300	31.6	8.04	4.37	92.02
MT-120–1300	33.4	8.29	3.73	90.99

For more detailed investigation of the structural changes due to mechanical activation, Raman mode of anatase at ~142 ($E_{g(1)}$) and TiO_2 II mode at ~338 cm^{-1} are particularly analized [19]. In the Fig. 2 full width at half maximum (FWHM) is shown for modes mentioned above as a function of milling time. A growth of $E_{g(1)}$ linewidth for the period of activation longer then 5 min (Fig. 2(a)), together with the decrease in the intensity and broadening of all anatase modes (Fig. 1) can be explained by fragmentation of anatase grains and introducing defects during treatments. Note also that the appearance of new TiO_2 phases, srilankite and rutile (wich acording to the literature have Raman modes at about 151 cm^{-1} [15] and ~143 cm^{-1} [13], respectively), can influences the broadening of the Raman feature at ~142 in the powders activated for more than 40 min. On the other hand, mode of TiO_2 II (Fig. 2(b)) exhibits completely different trend: FWHM of this mode decreases with activation time for the treatment shorter than 80 min, but starts to increase for longer activation time. Such behavior points out not only to formation and gradual ordering of TiO_2 II phase at the beginning of activation, but also to the fragmentation and disorder of this phase that begins after 80 min of milling.

The nitrogen sorption isotherms are very similar shape for all samples. According to the IUPAC recommendation for classification of adsorption isotherms, obtained isotherms are corresponding to Type II isotherms, whereas the hysteresis loops can be classified as Type H1 [20]. Nitrogen adsorption/desorption isotherms for sample MT-0 and MT-120 are presented in Fig. 3.

The results obtained by N_2 sorption measurements are summarized in Table 2. An unusual behavior may be noticed: specific surface area, as well as total pore volume, decreases with milling time, reaching minimum values of 5.5 m^2/g and 0.029 cm^3/g respectively, and after 80 min starts to increase. There are few possible reasons which can contribute to the reduce of specific surface area (SSA) for approximately 65%. An irregular morphology of MgO can be observed in SEM micrograph of MT-0, whereas TiO_2 has smaller spherical particles (Fig. 4). The decrease in BET surface area may be associated to the agglomeration of small unstable TiO_2 particles. The irregular morphology of MgO was broken during the milling process and the pore structure destructed [21,22], which could also lead to decrease in SSA owing to cold welding of MgO attired particles. Furthermore, the reason for unexpected behavior of SSA can be related to the disappearance of anatase and appearance of new phase of TiO_2 II (Fig. 2(b)), having lower SSA than starting oxides. After 40 min of activation, the new phase starts to create in the form of larger particles produces greater SSA. Due to longer time of milling treatment these particle start to behave like the mechanical activation and fragmentation is at the beginning.

The microstructure analyses of MgO–TiO_2 system have showed that the initial MgO powder consisted of irregularly shaped agglomerates with a size of 2 microns approximately and spherical particles TiO_2 with size of 150 nm. For the activated samples, formation of soft agglomerates has been noticed as a formation of new phase, because of mechanically induced particles deforma-

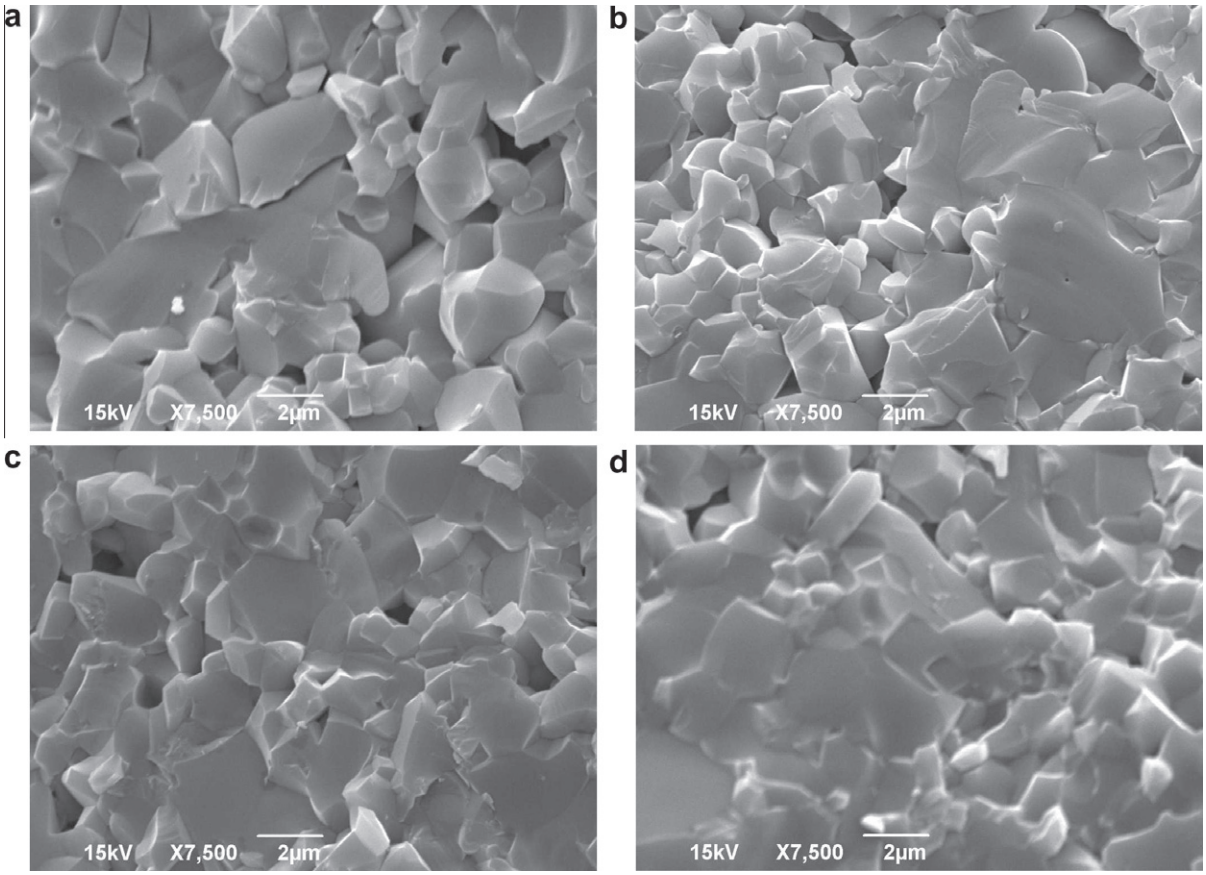

Fig. 6. SEM micrographs of samples (a) MT-0–1300, (b) MT-20–1300, (c) MT-80–1300 and (d) MT-120–1300.

tion, which is in agreement with Raman spectroscopy. The micrograph of the sample MT-80 indicates particle fragmentation.

The Raman spectra of the samples obtained by sintering non-milled and milled powders at 1300 °C are shown in Fig. 5. During the treatment at a higher temperature, two phased sistem ($MgTiO_3$ and Mg_2TiO_4) is formed [23]. According to the factor group analyses, $MgTiO_3$ there are ten Raman active modes $5A_g + 5E_g$, whereas spinel Mg_2TiO_4 has five ones ($A_{1g} + E_g + 3F_{2g}$). All ten bends corresponding to $MgTiO_3$ were observed in the Raman spectra of sintered samples at the following position: 225 cm^{-1} (A_g), 282 cm^{-1} (E_g), 307 cm^{-1} (A_g), 353 cm^{-1} (E_g), 398 cm^{-1} (A_g), 485 cm^{-1} (E_g), 504 cm^{-1} (A_g), 638 cm^{-1} (E_g), ~725 cm^{-1} (A_g) [24,25]. On the other hand, it is hard to resolve the Raman modes that originated from Mg_2TiO_4 phase, as they are at the similar positions as the modes of $MgTiO_3$ and partially overlapped with them [26]. Besides, an additional Raman feature, noticed at 596 cm^{-1}, is assigned to $MgTiO_3$ II. These high-pressure $MgTiO_3$ phase with the lithium-neonate structure may be metastable quench phase of perovskite [8].

As it can be seen from Fig. 5(a), all Raman spectra of sintered samples are almost identical, considering the number and position of the main features. The only difference observed is in the realative intensity and shape of some features, and special attention is dedicated to the analysis of the Raman feature at about 720 cm^{-1}. Deconvolution of this feature by two separated Lorentzian shape peaks using last–squares optimization method for sintered samples is shown in Fig. 5(b). The positions of these peaks in all spectra are at ~713 and ~730 cm^{-1}, but their intensity ratio varies. First of these peaks at ~713 cm^{-1} can be Raman mode ascribed to the vibrations of O atoms in TiO_6 octahedrons of ordered $MgTiO_3$ structure [27]. The appearance of the mode at ~730 cm^{-1} indicates the presence of structural order–disorder at short-range, suggesting the presence of [TiO_5] complex clusters and defects (oxygen vacancies) introduced by mechanical activation and subsequent sintering [27]. Note that [TiO_6] and [TiO_5] complex clusters in the sintered samples studied here can also belong to the Mg_2TiO_4 structure. So, the intensity ratio of the Raman features at ~713 and ~730 cm^{-1}, presented in Fig. 5(c), can be use as an indicator of structural ordering and concentration of oxygen vacancies. This indicates that mechanical activation before sintering can decrease the concentration of oxygen vacancies into the lattice, resulting in a more ordered structure of sintered samples. However, the activation is able to increase the degree of structural order into the lattice just for shorter activation time (up to 80 min), whereas extension of this process is associated with structural disorder.

Values of electrical measurements, dielectric permittivity (ε_r), loss tangent (tgδ) and specific resistance (ρ, given in Ωcm) as well as densities obtained after sintering (d, given in percents of theoretical density) as a function of time of mechanical treatment are given in Table 3. The resultes pointed out that the dielectric permittivity of these specimens increase with activation time. Also it is known from the literature data that different ratio between phases has influence in ε_r values [6]. It is believed that the densities play an important role in controlling dielectric loss. The tgδ value is generally affected not only by the lattice vibration modes, but also by the pores, the second phases, the impurities, the lattice defect, crystallizability and inner stress [28]. The increase in activation time is beneficial to the densification after sintering and crystallizability until the loss tangent value reaches the minimum. The further increase in activation time is result in the appearance of abnormal grains and pores after sintering process and consequently leads to the increase of the tgδ value [29]. Specific resistance increase with milling time until 80 min is probably induced with existence large crack between areas. Sample MT-

120–1300 has more compact structure and consequently lower values of specific resistance.

Micrographs of samples sintered at 1300 °C for 2 h indicate medium sintering stage along with enclosed but not spherical pores and two different phases, Fig. 6, which is in accordance with results obtained with Raman spectroscopy. Presence of fracture between grains, which is due to presence of agglomerates in starting powders, was noticed. Observing morphology of MT-120–1300, may be noted that it is the most homogeneous structure, which cause the higher values of dielectric constant.

4. Conclusion

In this article the influence of ball miling process on the structure of $MgO–TiO_2$ system, along with its influence on electrical properties of post-sintering samples was investigated. The Raman spectroscopy of activated powers pointed out phase transition of anatase, through high pressure TiO_2 II and srilankite, to the most stabile rutile phase. In addition, the mechanical strain have led to the small blue shift of low-frequency modes of anatase and TiO_2 II, whereas the intensity decrease and broadening of anatase bands have been the consequences of grain fragmentation and introducing defects during the mechanical activation. The results obtained by nitrogen adsorption are in agreement with those obtained by Raman, as well as SEM measurements.

The Raman spectroscopy, like as scanning electron microscopy of sintered samples, points out to structural modifications depending on duration of mechanical activation before sintering process. The variation in the Raman spectra of the sintered samples indicates that mechanical treatment decreases concentration of oxygen vacancies and increases the degree of structural order for activation time up to 80 min. Moreover, the structural ordering is followed by increasing density and reducing dielectric loss tangent of sintered samples. The most ordered sample MTS-80 with maximal density has minimal value of dielectric loss tangent, which makes it a good candidate for application in electronic industry.

This study has shown that mechanical activation and subsequent sintering, with proper choice of processing parameters, can improve the structural and electrical properties of sintered magnesium-titanate ceramics.

Acknowledgement

This research was performed within project 172057 OI financed by the Ministry for Education and Science of the Republic of Serbia.

References

[1] A. Belous, O. Ovchar, D. Durilin, J. Am. Ceram. Soc. 89 (2006) 3441–3445.
[2] Z. Li, S. Chun-Ying, Q. Tai, J. Inorg. Mater. 26 (2011) 219–224.
[3] N. Stubičar, A. Tonejc, M. Stubičar, J. Alloys Comp. 370 (2004) 296–301.
[4] M.K. Suresh, J.K. Thomas, H. Sreemoolanadhan, C.N. George, A. John, S. Solomon, P.R.S. Wariar, J. Koshy, Mater. Res. Bull. 45 (2010) 761–765.
[5] A. Belous, O. Ovchar, D. Durylin, M. Valant, M. Macek-Krzmanac, D. Suvorov, J. Eur. Ceram. Soc. 27 (2007) 2963–2966.
[6] E.S. Kim, S.N. Seo, J. Korean Ceram. Soc. 47 (2010) 163–168.
[7] J. Zabicky, G. Kimmel, E. Goncharov, F. Guirado, Z. Kristallogr. Suppl. 30 (2009) 347–352.
[8] J.A. Linton, Y. Fei, A. Navrotsky, Am. Mineral. 84 (1999) 1595–1603.
[9] H.St.C. O'Neill, D.R. Scott, Eur. J. Mineral. 17 (2005) 315–323.
[10] H. Kang, L. Wang, D. Xue, K. Li, C. Liu, J. Alloys Comp. 460 (2008) 160–163.
[11] S. Filipovic, N. Obradovic, V.B. Pavlovic, S. Markovic, M. Mitric, M.M. Ristic, Sci. Sinter. 42 (2010) 143–151.
[12] T. Ohsaka, F. Izumi, Y. Fujiki, J. Raman Spectrosc. 7 (1978) 321–324.
[13] M. Rezaee, S.M.M. Khoie, K.H. Liu, CrystEngComm 13 (2011) 5055–5061.
[14] G.A. Tompsett, G.A. Bowmaker, R.P. Cooney, J.B. Metson, K.A. Rodgers, J.M. Seakins, J. Raman Spectrosc. 26 (1995) 57–62.
[15] H. Dutta, P. Sahu, S.K. Pradhan, M. De, Mater. Chem. Phys. 77 (2002) 153–164.
[16] A. Gajović, M. Stubičar, M. Ivanda, K. Furić, J. Mol. Struct. 563–564 (2001) 315–320.
[17] R.G. Schlecht, H.K. Bockelmann, Phys. Rev. Lett. 31 (1973) 930–932.
[18] M. Šćepanović, S. Aškrabić, V. Berec, A. Golubović, Z. Dohčević-Mitrović, A. Kremenović, Z.V. Popović, Acta Phys. Pol., A 115 (2009) 771–774.
[19] X. Pan, X. Ma, J. Solid State Chem. 177 (2004) 4098–4103.
[20] S.J. Greg, K.S. Sing, Adsorption Surface Area and Porosity, Academic Press, London/New York, 1967.
[21] A. Rougier, S. Soiron, I. Haihal, L. Aymard, B. Taouk, J.M. Tarascon, Powder Technol. 128 (2002) 139–147.
[22] T. C. Alex, R. Kumar, A. J. Kailath, S. K. Roy, S. P. Mehrotra, Physicochemical changes during mechanical activation of boehmite, Proceedings of the XI International seminar on Mineral Processing Technology (MPT-2010) 898–904.
[23] N. Obradović, S. Filipović, V.B. Pavlović, A. Maričić, N. Mitrović, I. Balać, M.M. Ristić, Sci. Sinter. 43 (2011) 145–151.
[24] C.H. Wang, X.P. Jing, W. Feng, J. Lu, J. Appl. Phys. 104 (2008) 034112–034112-6.
[25] T. Hirata, K. Ishioka, M. Kitajima, J. Solid State Chem. 124 (1996) 353–359.
[26] S. Kumar, R. Kumar, B.H. Koo, H. Choi, D.U. Kim, C.G. Lee, J. Ceram. Soc. Jpn. 117 (2009) 689–692.
[27] E.A.V. Ferri, J.C. Sczancoski, L.S. Cavalcante, E.C. Paris, J.W.M. Espinosa, T. de Figueiredo, P.S. Pizani, V.R. Mastelaro, J.A. Varela, E. Longo, Mater. Chem. Phys. 117 (2009) 192–198.
[28] W. Lei, J.H. Zhu, X.H. Wang, Mater. Lett. 61 (2007) 4066–4069.
[29] N. Obradović, S. Filipović, V. Pavlović, V. Paunović, M. Mitrić, M.M. Ristić, Acta Phys. Pol., A 120 (2011) 322–325.